

Article

Spin-Trapping Analysis of the Thermal Degradation Reaction of Polyamide 66

Akihiro Kurima ^{1,2}, Kenji Kinashi ³ , Wataru Sakai ^{3,*} and Naoto Tsutsumi ³ 

¹ Doctor's Program of Materials Chemistry, Graduate School of Science and Technology, Kyoto Institute of Technology, Matsugasaki Sakyo, Kyoto 606-8585, Japan

² Platform Laboratory for Science & Technology, Asahi-Kasei Corporation, Moriyama City 524-0002, Japan

³ Faculty of Materials Science and Engineering, Kyoto Institute of Technology, Kyoto 606-8585, Japan

* Correspondence: wsakai@kit.ac.jp; Tel.: +81-75-724-7818

Abstract: The radical mechanisms of the thermal degradation of polyamide 66 (PA66) occurring under a vacuum at a temperature range between 80 °C and 240 °C (which includes the temperature of practical applications) were investigated using a spin-trapping electron spin resonance (ST-ESR) technique, as well as FTIR, TG-DTA, and GPC methods. No significant weight loss and no sign of thermal degradation are observed at this temperature range under oxygen-free conditions, but a slight production of secondary amine groups is confirmed by FTIR. GPC analysis shows a small degradation by the main chain scission. ST-ESR analysis reveals two intermediate radicals which are produced in the thermal degradation of PA66: (a) a $\bullet\text{CH}_2$ radical generated by main chain scission and (b) a $-\bullet\text{CH}-$ radical generated by hydrogen abstraction from the methylene group of the main chain. The ST-ESR result does not directly confirm that a $-\text{NH}-\bullet\text{CH}-$ radical is produced, although this reaction has been previously inferred as the initiation reaction of the thermal degradation of PA; however, the presence of $-\bullet\text{CH}-$ radicals strongly suggests the occurrence of this initiation reaction, which takes place on the α -carbon next to the NH group. The ST-ESR analysis reveals very small levels of reaction, which cannot be observed by common analytical methods such as FTIR and NMR.

Keywords: polyamide 6,6 (PA66); nylon 66; thermal degradation; electron spin resonance (ESR); spin-trapping method; radical intermediates; 1,3,5-tri-*tert*-butyl-2-nitrosobenzene (TTBNB)



Citation: Kurima, A.; Kinashi, K.; Sakai, W.; Tsutsumi, N.

Spin-Trapping Analysis of the Thermal Degradation Reaction of Polyamide 66. *Polymers* **2022**, *14*, 4748. <https://doi.org/10.3390/polym14214748>

Academic Editors: Roberto Scaffaro and Emmanuel Fortunato Gulino

Received: 8 October 2022

Accepted: 2 November 2022

Published: 5 November 2022

Publisher's Note: MDPI stays neutral with regard to jurisdictional claims in published maps and institutional affiliations.



Copyright: © 2022 by the authors. Licensee MDPI, Basel, Switzerland. This article is an open access article distributed under the terms and conditions of the Creative Commons Attribution (CC BY) license (<https://creativecommons.org/licenses/by/4.0/>).

1. Introduction

Degradation is an unavoidable problem affecting resin materials used in industry. For example, microplastics are a worldwide environmental problem [1–3] caused by the fragmentation of plastics as a result of degradation [4,5]. Plastic materials are cheaper, lighter, and easier to form than metals and ceramics, which have been used since ancient times. However, plastics are far less resistant to light and heat than these materials, thus, anti-degradation agents are commonly added to plastics to extend their life. It is desirable to select the best anti-degradation agent based on the degradation mechanism for each material; however, in practice, in material development, different anti-degradation agents are often tested through trial and error based on experience. This approach does not always result in a logical solution based on the degradation mechanism that actually affects the materials. One of the reasons for this shortcoming is that degradation is made up of multi-step reactions, including chain reactions, which makes the analysis of the reaction mechanism complex and difficult. Moreover, as many textbooks and papers assert, the degradation of polymer materials proceeds through radical reactions, which, however, cannot be observed by common analytical methods such as FTIR and NMR. Generally, reaction analysis is performed by measuring a sample after degradation, using, for example, Fourier transform infrared spectroscopy (FTIR). However, with this method, it is necessary to estimate the radical reaction path from the final products after degradation, and thus,

the exact path, including radical species, may not be known directly. In addition, due to the sensitivity limits of the analysis, changes in chemical structures cannot be detected unless the sample has been significantly degraded, which makes the estimation of the initial reaction pathway particularly difficult.

Generally, degradation reactions are caused by light, heat, and mechanical fatigue, and most proceed through radical reactions that break polymer chains. Among the many analytical methods, electron spin resonance (ESR) is the only method that can detect radicals, and its high sensitivity enables the capture of the initial stage of degradation. However, because organic radicals are generally very unstable and their lifetimes are often counted in milliseconds or less, the detection of the radical intermediates of polymer degradation by ESR is also difficult [6–8]. There are methods for dealing with short-lived species using pulsed ESR measurements and cryogenic cooling methods with suppression of reaction processes, but each method has its own problems in that the equipment is extremely expensive, the species observed are limited, and the measurement conditions do not reflect the actual degradation environment.

To address these serious problems, our laboratory focused on the spin-trap method to convert short-lived organic radicals into stable radicals [9–12]. The pre-added spin-trapping reagent captures free radicals to form persistent radicals called spin adducts, which are detectable by standard ESR equipment using a continuous-wave method. The detailed analysis of the ESR spectra of the spin adducts allows the intermediate radicals to be determined as they originate from thermal degradation reactions in various polymer materials, such as poly(butylene terephthalate) [13], thermoplastic elastomer [14], poly(vinyl alcohol) [15], and poly(propylene) [16].

In this study, we attempted to analyze the radicals generated in the thermal degradation of polyamide 6,6 (PA66), a common engineering plastic that is also known as nylon 66, using a spin-trapping ESR (ST-ESR) technique. Polyamide (PA) is widely used in automobile engine parts because of its excellent heat resistance. However, there is a need to further improve its heat resistance so that it can be used in more severe conditions over a longer period. The mechanism of thermal degradation of PA66 has been studied since the 1950s. Subsequent studies, however, have yielded different results depending on degradation conditions; these studies have been reviewed in detail by Levchik, et al., in 1999 [17], and elsewhere [18–20]. These differences come about because there are many secondary reactions involved in the thermal degradation of PA66; as a result, the thermal degradation mechanism of PA66 is not well understood. However, most reports agree that degradation begins with hydrogen abstraction or detachment from the methylene group at the β -position of the carbonyl group ($-\text{CH}_2-\text{CH}_2-\text{CO}-\text{NH}-$) or adjacent to the NH ($-\text{CH}_2-\text{NH}-\text{CO}-$). That said, these analyses are based on decomposition at high temperatures above 350 °C or conventional processing temperatures above melting point [21,22]; there are few reports on degradation at temperatures around 200 °C or lower than the melting point of PA66 [23–25], to which automotive and other practical parts are routinely exposed. Although the decomposition temperature at which PA shows an obvious decrease in its molecular weight is 400 °C or higher, the thermal oxidative degradation of PA66 progresses at lower temperatures, as evidenced by the decline in its physical properties when a 100 μm thick film is held at 100 °C for a long period [25]. Therefore, it is very important to understand the details of the degradation mechanism of PA66 at lower temperatures of around 200 °C or less. Although a few cases using radical generation by γ -irradiation or mechanochemistry have been analyzed [26–28], no studies of radicals have examined the thermal degradation of PA because intermediate radicals are quickly quenched at or above room temperature. Thus, in this paper, the thermal degradation of PA66 molecules was studied using ST-ESR by analyzing radical generation during the heating processes, firstly under oxygen-free conditions.

2. Materials and Methods

2.1. Materials

The materials used for the spin-trapping experiments presented in this study are shown in Figure 1. PA66 was synthesized by polycondensation from the nylon salts constituted with adipic acid and hexamethylenediamine at 285 °C under a vacuum of 20 Pa and then purified by reprecipitation with 1,1,1,3,3,3-hexafluoro-2-isopropanol (HFiP)/methanol. The weight average molecular weight, M_w , of the obtained PA66 measured by GPC was 43,600. The spin-trapping reagent was 1,3,5-tri-*tert*-butyl-2-nitrosobenzene (TTBNB), which was purchased from Tokyo Chemical Industry Co., Ltd. (Tokyo, Japan); HFiP and methanol were purchased from Fluorochem Ltd. (Derbyshire, UK) and FUJIFILM Wako Pure Chemical Co. (Osaka, Japan), respectively.

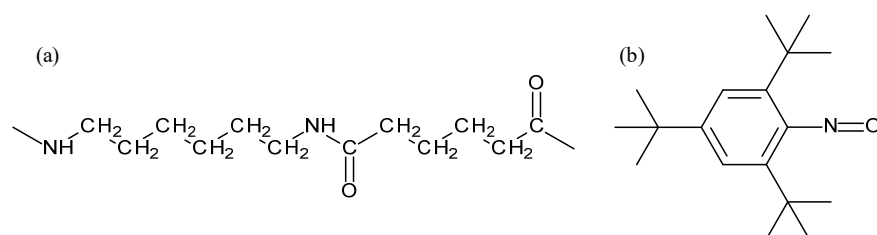


Figure 1. Materials used in this study: (a) PA66 and (b) spin-trapping reagent 2,4,6-tri-*tert*-butylnitroso-benzene (TTBNB).

2.2. Sample Preparation

PA66 purified by reprecipitation and the spin-trapping agent were dissolved in HFiP and cast on a glass plate. After air-drying, the residual solvent in PA66 was removed in a vacuum dryer at 50 °C for 3 h. The concentration of TTBNB in the PA66 matrix was controlled at 3 wt%. The thickness of the film was ca. 500 μm .

2.3. Characterization

2.3.1. TG-DTA Measurements

Weight loss and differential thermal analysis versus temperature were obtained using a thermal gravimetric-differential thermal analysis (TG-DTA) apparatus (TG/DTA6200, Hitachi High-Tech Science Co. (Tokyo, Japan)). Approximately 5 mg of the PA66 sample was placed on an aluminum pan and heated from room temperature (RT) to 600 °C at a rate of 10 °C/min under a nitrogen gas flow of 50 mL/min.

2.3.2. GPC Measurements

Molecular weight (MW) distribution changes in the PA66 were measured before and after heating, using a gel permeation chromatography (GPC) system (HLC-8320GPC, Tosoh Co. (Tokyo, Japan)) with three columns of TSKgel (GMH_{HR}-H(S), Tosoh Co. (Tokyo, Japan)) connected in series. MWs were calibrated using poly(methyl methacrylate) standards. The PA66 samples were dissolved in HFiP solution and then filtered using a 0.45 μm -sized pore membrane. The injected sample concentration of PA66 was 0.1 wt%. In each measurement, a sample of 10 μL was injected at a flow rate of 0.175 mL/min. The temperatures of the columns and the RI detector were maintained at 40 °C continuously. The number average MW, M_n , and the weight average MW, M_w , were calculated from the distribution curve.

2.3.3. FTIR Measurements

Fourier-transform infrared spectroscopy (FTIR) was performed using a transmission method (IR-670, Agilent Technologies, Inc. (Santa Clara, CA, USA)). All the spectra were recorded with the wavenumber in the range 4000 cm^{-1} to 400 cm^{-1} at a resolution of 2 cm^{-1} by averaging 256 scans. A thin PA66 film of approximately 10 μm for FTIR was prepared by casting method using HFiP.

2.3.4. ESR Measurements

ESR measurements were carried out on an ESR spectrometer (E500, Bruker Co. (Billerica, MA, USA)) using an X-band microwave at a frequency of approximately 9.5 GHz and a power of 1.0 mW. The magnetic field was around 3300 G, and the modulation width was 1 G at 100 kHz. Cr^{2+} was used as an external standard for radical amounts. The 70 mg of PA66 with TTBNB was placed and sealed in a 5 mm diameter quartz ESR test tube under vacuum condition. The heating temperature was controlled precisely from RT to 240 °C with a thermal controller unit (DVT3000, Bruker Co. (Billerica, MA, USA)). The obtained ESR spectra were carefully simulated, separated, and qualified using a personal computer and commercial software (Igor Pro, WaveMetrics Inc. (Portland, OR, USA)). The multiple peak ESR spectra were simulated using mixed Gaussian–Lorentzian functions for all peaks with different spectral parameters, including the center field, the integrated intensity of the peak area, the peak-to-peak width, and the Gaussian–Lorentzian ratio.

3. Results and Discussion

3.1. TG-DTA of PA66

The thermal stability of PA66 was evaluated by measuring weight loss, as well as heat flow in and out using TG-DTA at a heating rate of 10 °C/min under an inert nitrogen atmosphere. As shown in Figure 2, there was a weight loss of about 8% at 250 °C in the TGA curve. This loss is not attributed to thermal degradation but mainly to the volatilization of water and low molecular weight components generated during polymerization because the DTA curve shows only a featureless, endothermic curve over this temperature range. The endothermic peak at 261 °C in the DTA curve is attributed to the melting of crystalline PA66 [29]. Although significant thermal decomposition can be observed from 350 °C to 450 °C in the TGA curve, no peak and no apparent curvature change due to the thermal decomposition is observed below 330 °C, which includes the temperature range in which ESR measurement was performed. DTA showed an endotherm peak between 350 °C and 450 °C; this is considered to be due to a decrease in the heat capacity of the sample and the evaporation of volatile components [21] caused by rapid weight loss from thermal decomposition.

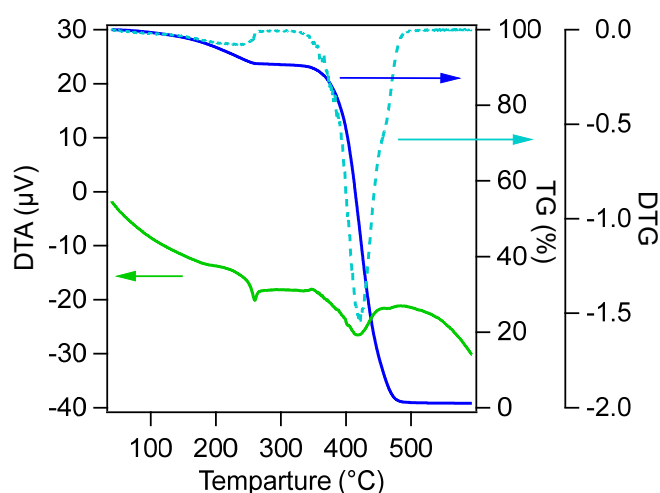


Figure 2. DTA and TG curves for PA66 at a heating rate of 10 °C/min under inert nitrogen atmosphere. The DTG curve was obtained by differentiating the TG curve.

3.2. Thermal Degradation Analysis with GPC

The MW of PA66 was compared before and after heating using the same stepwise heating profile of ESR measurement under vacuum conditions. The M_n , M_w , and the degree of dispersion (M_w/M_n) are summarized in Table 1. Degradation did not progress significantly, even when the sample was heated at a temperature below 240 °C; this is

thought to be because of the short heating time and the lack of oxygen. However, there was a slight decrease in M_n , and MW dispersion was slightly greater after heat treatment. These changes suggest that the results of the ESR measurements in the latter section show the reactions in the very early stages of thermal degradation.

Table 1. The average molecular weights of PA66 before and after heating, as determined by GPC measurement.

Condition	M_n	M_w	M_w/M_n
Not heated	15,600	43,600	2.79
After heating	14,200	43,500	3.06

3.3. Thermal Degradation Analysis with FTIR

FTIR analysis was performed to investigate chemical structural changes caused by thermal degradation at a low temperature range below 200 °C. In the ESR analysis described in the next section, each ESR spectrum was taken over 4 min during stepwise heating of the sample, for 50 min until the temperature reached 240 °C. However, because a change of at least a few percentage points was required to detect a distinct difference between FTIR spectra before and after degradation, the PA66 samples had to be heated for a longer time, of the order of 10 h. Figure 3 shows the FTIR spectra of PA66 before and after heating at 160 °C for 13 and 82 h under vacuum conditions. It can be seen that there is little noticeable degradation in progress. However, a detailed comparison reveals a slight increase in amino groups in the 3300 cm^{-1} region. On the other hand, there are no significant changes in the region of carbonyl groups in the 1500–1700 cm^{-1} region, suggesting that, while peroxidative degradation did not proceed because of the non-oxidative condition, main chain scission between the amide group and the adjacent carbons, $-\text{CO}-\text{NH}-\text{CH}_2-$, may have occurred, resulting in the formation of secondary amines.

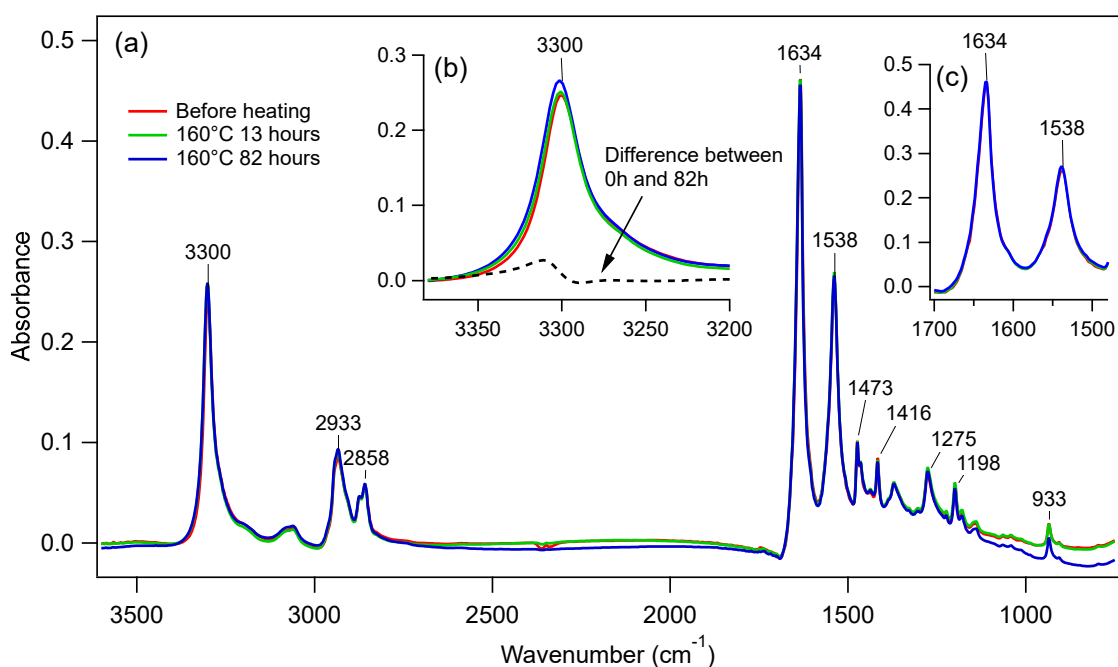


Figure 3. (a) FTIR spectra of PA66 before and after heating at 160 °C for 13 h and 82 h, and enlarged spectra; (b) amine group region around 3200–3600 cm^{-1} with difference spectrum; and (c) carbonyl group region around 1450–1700 cm^{-1} .

3.4. Radical Analysis by Spin-Trapping ESR

3.4.1. ESR Measurements

The results of ESR measurements of PA66, including the spin-trapping reagent TTBNB sample with stepwise heating at 20 °C intervals, are shown in Figure 4. A slight ESR signal can be observed at the center from 80 °C, and it increases with increasing temperature with other signals; the spectral intensity finally reaches a maximum at 220 °C. Then, the signals suddenly almost disappear at 240 °C. Similar measurements on PA66 without TTBNB did not show any ESR signals. Therefore, the signals observed in Figure 4 were spin adducts resulting from the trapping of radical intermediates generated from PA66 as a result of thermal degradation. To separate the spin adducts and to determine from which radicals they originate, computational simulation analysis for all spectra observed in Figure 4 was performed.

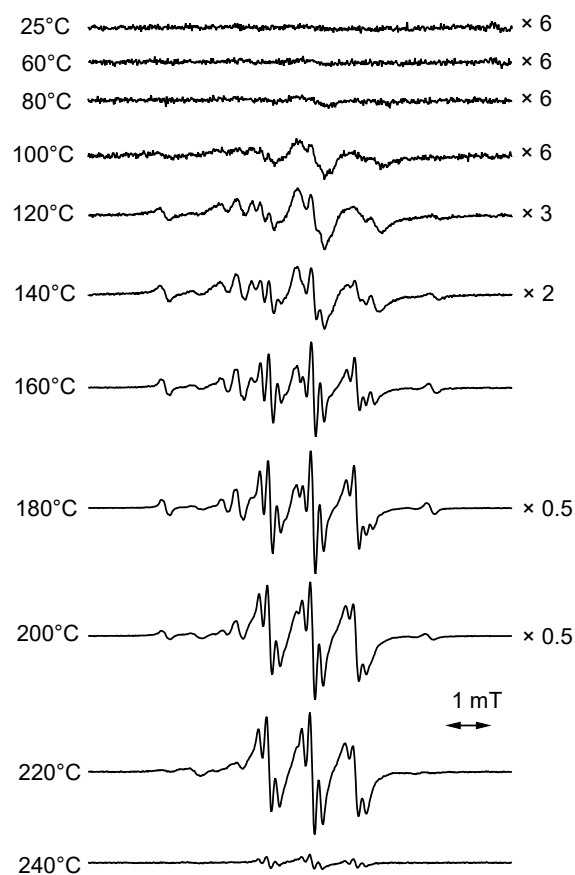


Figure 4. ESR spectra of PA66/TTBNB during stepwise heating from RT to 240 °C at 20 °C intervals.

3.4.2. Assignments of Spin Adducts

After elaborate trial and error analyses of the estimation of the produced radical species and the assumption of their spectral parameters, it was concluded that the spectrum consists of a maximum of six spin adduct components. Figure 5 shows an example of a simulation analysis of a spectrum heated to 160 °C, in which all six components can be observed. The assignments of the spin adduct radicals and their hyper coupling constant ($hfcc$) and g -values are shown in Table 2, together with the literature references for assignment.

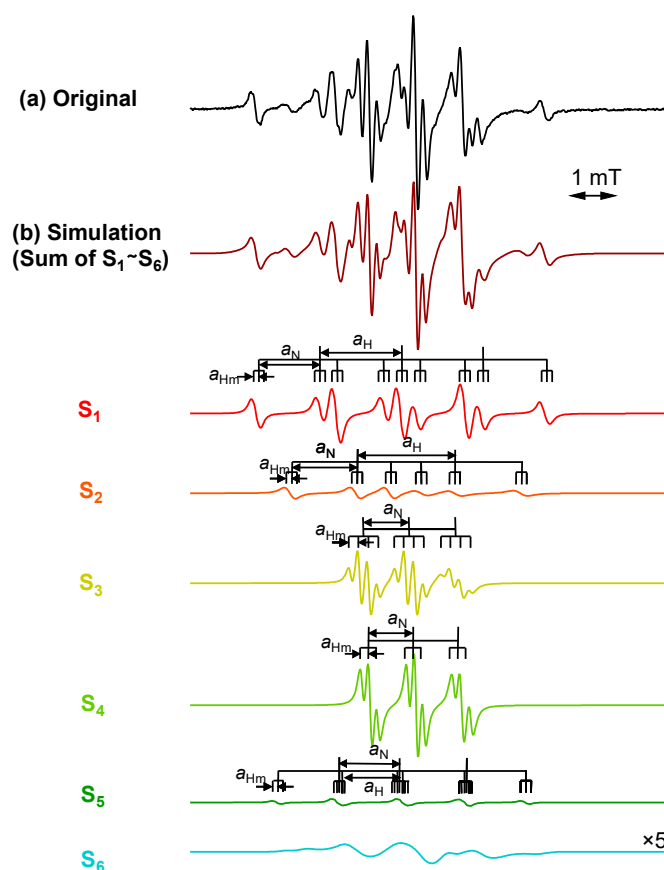


Figure 5. (a) ESR spectrum of PA66 with TTBNB observed at 160 °C on stepwise heating, and (b) simulated spectrum using six spin adduct components, S_1 – S_6 . The parameters a_{Hm} , a_N , and a_H are the hyperfine coupling constants (*hfcc*).

S_1 , which shows a 9-line feature, indeed consists of 27 lines with overlapping constructed by the interaction of three types of atoms: one nitrogen, two hydrogen on carbon, and two aromatic *m*-hydrogens. S_1 was assigned a nitroxide-type spin adduct derived from $\bullet\text{CH}_2\text{—CH}_2\text{—}$, which was produced by main chain scission [30]. It should be noted that this spin adduct should have at least two consecutive CH_2 groups because, if the substituent adjacent to $\bullet\text{CH}_2\text{—}$ is an amide group NH or a carbonyl group C=O , the value of *hfcc* is a little smaller compared with a simple hydrocarbon group [31].

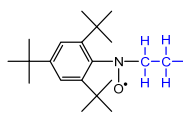
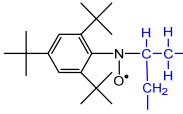
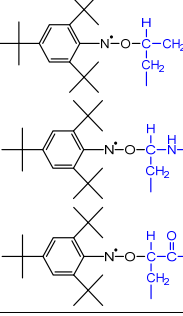
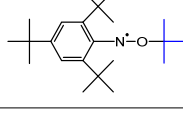
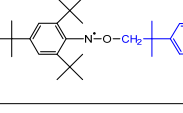
S_2 consists of 18 lines derived from one nitrogen, one hydrogen on carbon, and two aromatic *m*-hydrogen atoms. S_2 was assigned to a nitroxide-type spin adduct generated by trapping $\text{—}\bullet\text{CH—}$ produced by hydrogen abstraction from the methylene chain [32]. Given the value of a_H , the groups on both sides of $\text{—}\bullet\text{CH—}$ were considered to be methylene groups.

S_3 has a 12-line structure, consisting of 18 lines generated by trapping $\text{—}\bullet\text{CH—}$ as well as S_2 ; however, S_3 was assigned to an anilino-type. The *hfccs* of both β -hydrogen and *m*-hydrogens were almost equivalent. The *hfcc* of this anilino-type adduct is known to be unaffected by the chemical structure of the adjacent group of —CH— . The neighboring group has three candidates: methylene, or carbonyl, or amine in the amide group, but, as discussed below, it is most likely to be an amine [31].

S_4 with a nine-line structure was assigned to an anilino-type spin adduct produced by trapping the tertiary butyl carbon radical $\bullet\text{C}(\text{CH}_3)_3$ derived from the thermal degradation of TTBNB [33]. This spin adduct always appears when TTBNB is used and heated over 150 °C and exhibits a low *g*-value of 2.0033, which is easily distinguishable from the other components. S_5 was assigned to a self-trapping spin adduct derived from $\bullet\text{CH}_2\text{—}$ of the methyl group of TTBNB [16]. The component appears to show a 5-line structure with

overlapping, but actually consists of 27 lines and is observed only at a high temperature above 160 °C.

Table 2. The molecular structure of the assigned spin adducts, S₁–S₆, and their ESR spectral parameters observed for PA66 with TTBNB heated from RT to 240 °C, as well as the literature referred to in assigning the spin adducts.

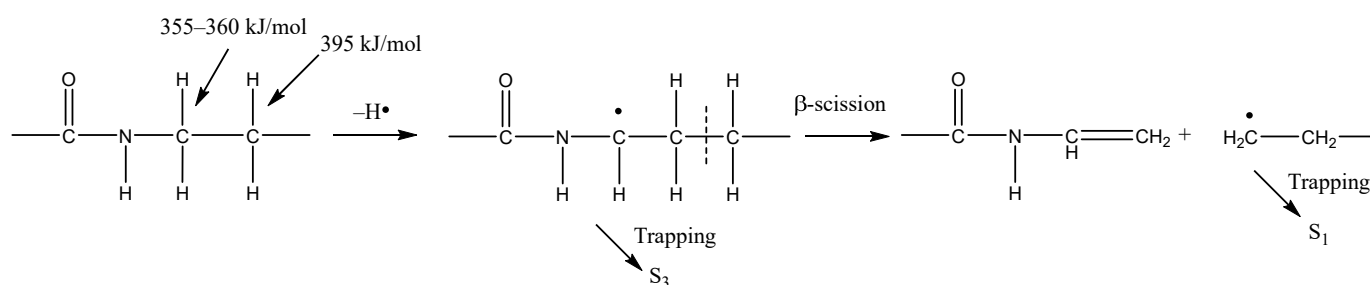
Observed Spin Adducts in This Paper				Referred Assignments in Previous Articles			
Assigned Molecular Structure	<i>hfcc</i> and <i>g</i>		Trapped Radical	<i>hfcc</i> and <i>g</i>		Materials	Ref.
S ₁ 	<i>a</i> _H (2)	1.75	•CH ₂ CH ₂ –	<i>a</i> _H (2)	1.799	<i>n</i> -Bu) ₃ Sn-Br(or I) /TTBNB/benzene	[30]
	<i>a</i> _N	1.40		<i>a</i> _N	1.346		
	<i>a</i> _{Hm}	0.08		<i>a</i> _{Hm}	0.083		
	<i>g</i>	2.0053		<i>g</i>	2.0060		
S ₂ 	<i>a</i> _H (1)	2.17	–•CH–CH ₂ –	<i>a</i> _H (1)	2.16	<i>n</i> -C ₁₂ C ₂₆ (paraffin) /TTBNB	[32]
	<i>a</i> _N	1.43		<i>a</i> _N	1.33		
	<i>a</i> _{Hm}	0.08		<i>a</i> _{Hm}	N/A		
	<i>g</i>	2.0046		<i>g</i>	2.0061		
S ₃ 	<i>a</i> _H (1)	0.20	–CH ₂ –•CH–CH ₂ –	<i>a</i> _H (1)	0.18	C ₆ H ₁₂ /(<i>tert</i> -BuO) ₂ /TTBNB/benzene	[30]
	<i>a</i> _N	1.00		<i>a</i> _N	1.10		
	<i>a</i> _{Hm}	0.20		<i>a</i> _{Hm}	0.18		
	<i>g</i>	2.0039		<i>g</i>	2.0036 ~ 2.0040		
S ₄ 	<i>a</i> _N	1.02	•C(CH ₃) ₃ (TTBNB)	<i>a</i> _N	1.05	<i>n</i> -eicosane /TTBNB	[33]
	<i>a</i> _{Hm}	0.17		<i>a</i> _{Hm}	0.193		
	<i>g</i>	2.0033		<i>g</i>	2.0046		
S ₅ 	<i>a</i> _H (2)	1.42	•CH ₂ – (TTBNB)	<i>a</i> _H (2)	1.46	PP/TTBNB	[16]
	<i>a</i> _N	1.29		<i>a</i> _N	1.05		
	<i>a</i> _{Hm}	0.08		<i>a</i> _{Hm}	0.10		
	<i>g</i>	2.0052		<i>g</i>	2.0054		
S ₆ <i>unassigned</i>	<i>a</i> _H	N.A.		<i>a</i> _H	–	N.A.	
	<i>a</i> _N	1.3–1.5		<i>a</i> _N	–		
	<i>a</i> _{Hm}	N.A.		<i>a</i> _{Hm}	–		
	<i>g</i>	2.0033		<i>g</i>	–		

S₆ is a broad component consisting of more than five peaks, with no clear hyperfine structure observed by wide broadening. S₆ is probably a macro-radical with low molecular mobility, which is fixed at the interface between the crystalline and amorphous phases of PA66. Since this broad component was also apparent in the spectrum for the sample heated at 80 °C, it may be a degradation sub-product radical originating from peroxides which have been produced before ESR measurement. The *g*-value of S₆ is 2.0033, and the *hfcc* of about 1.3–1.5 mT and 5–7 lines can be roughly read out from this structure. This is most likely a spin adduct derived from an alkyl radical. However, the true structure of S₆ is currently unknown; it was not possible to observe a more detailed *hfcc* for this component.

3.5. Reaction Mechanism of PA66 Thermal Degradation

This discussion of degradation mechanisms is based on ST-ESR and other analytical results. First, it should be noted that the temperature range, from RT to 240 °C, used in this study was relatively low compared with previous studies of PA66. There is no significant

weight loss up to 240 °C, as shown by TG-DTA analysis (Figure 2), indicating that there is no production of volatile compounds, such as cyclopentanone or CO₂, in this temperature range as would occur with higher temperature pyrolysis [20]. This finding is confirmed by FTIR measurements (Figure 5) where no apparent spectral change is observed, other than a slight increase in amino group. From recent studies [25,34], it has been proposed and accepted that the initiation reaction in thermal oxidative degradation at 90–200 °C is a hydrogen abstraction (detachment) from the α -carbon methylene group next to the NH group, as shown in Scheme 1. This mechanism is based on the fact that the bond dissociation energy of C–H in the methylene group next to NH (355–360 kJ/mol) is lower than that of C–H in other methylene units (395 kJ/mol). If this methine radical ($-\text{NH}-\dot{\text{C}}\text{H}-$) is trapped by TTBNB, the S_3 component will be produced. Figure 6 shows the temperature dependence of radical generation for each spin adduct component. S_3 is generated from a low temperature of 100 °C and increases from 160 °C up to 200 °C. If oxygen is present around the PA66, the oxygen quickly adds on the carbon radical $-\dot{\text{C}}\text{H}-$ and subsequent degradation reactions via peroxidation and homolysis proceed, eventually cleaving the $\text{NH}-\text{CH}_2$ bond to produce secondary amines and aldehydes. However, if no oxygen is present, as in the case of our ESR measurements, $-\text{NH}-\dot{\text{C}}\text{H}-$ may directly proceed to two types of main chain scission by β -scission reactions: one produces $\dot{\text{C}}\text{H}_2-$ radicals and the other produces $-\dot{\text{C}}=\text{O}$ radicals, which were not detected by ST-ESR in this paper.



Scheme 1. Hydrogen abstraction of NH α methylene unit for the thermal degradation mechanism of PA66.

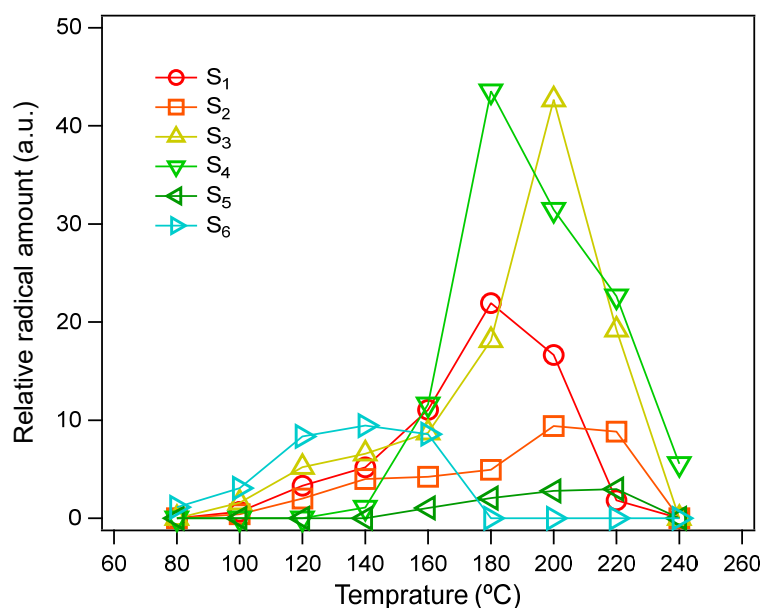
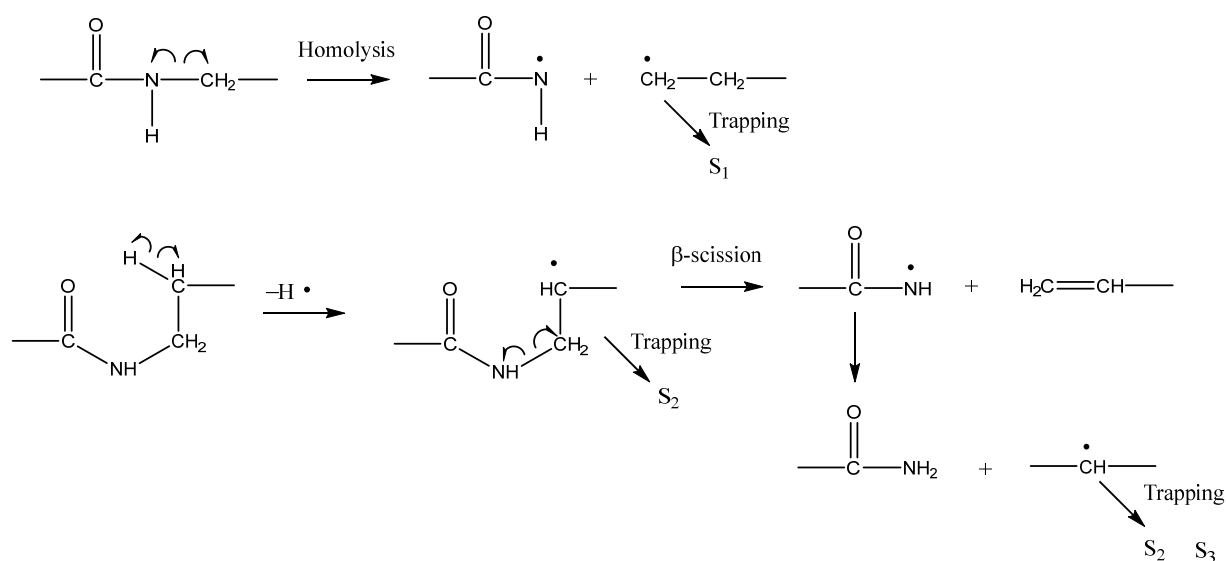


Figure 6. Radical amounts of spin adduct produced during stepwise heating of the PA66 sample.

For the production of the secondary amine radical in the thermal degradation of polyamide, two mechanisms have been proposed for temperatures higher than 300 °C,

which is much higher than the temperature conditions in our case: either main chain scission producing $\bullet\text{NH}-$ and $\bullet\text{CH}_2-$, or hydrogen abstraction from the β -methylene group to the NH group producing $\bullet\text{NH}-$ and $-\bullet\text{CH}-$ [17], as shown in Scheme 2. It has been reported that the bond dissociation energy on the bond $\text{NH}-\text{CH}_2$ is lowest in the PA66 molecular structure [35]; this leads to the assumption that main chain scission at $-\text{NH}-\text{CH}_2-$ is more likely in decomposition. Indeed, we observed a large amount of S_1 derived from $\bullet\text{CH}_2-$, as shown in Figure 6. In the case of the β -scission scheme, the main chain radical $-\bullet\text{CH}-$ is produced, which may be trapped and observed as the S_2 spin adduct. However, in our study, we could not detect a spin adduct derived from the amino radical $\bullet\text{NH}-$; this may be due to the high reactivity of the amino radical $\bullet\text{NH}-$ and low reactivity of TTBNB against a nitrogen radical.



Scheme 2. The secondary amide generation scheme for the thermal degradation mechanism of PA66.

4. Conclusions

The radical mechanism of thermal degradation of polyamide 66 (PA66) occurring under vacuum conditions at temperatures between 80 °C to 240 °C (which includes the temperature range of practical applications), was investigated mainly using a ST-ESR technique. Degradation analysis by TG-DTA on temperature ramp mode and FTIR after heating at 160 °C for 82 h shows no significant weight loss and no sign of oxidative degradation in this temperature range. However, a slight production of secondary amine groups was confirmed by FTIR. GPC analysis showed a small increase in molecular weight dispersion with a small decrease in average molecular weight. Changes in the molecular weight distribution indicate that main chain scission is the prevalent mechanism. ST-ESR analysis reveals that two intermediate radicals are produced via the thermal degradation of PA66: (a) a $\bullet\text{CH}_2-$ radical generated by main chain scission and (b) a $-\bullet\text{CH}-$ radical generated by hydrogen abstraction from the methylene group of the main chain. The ST-ESR did not directly confirm that a $-\text{NH}-\bullet\text{CH}-$ radical is produced by hydrogen abstraction or detachment, although this reaction had been inferred before as the initiation reaction of thermal degradation of PA at the relatively low temperature below 200 °C. However, the ESR analysis reveals the presence of $-\bullet\text{CH}-$ radicals and strongly supports the occurrence of this reaction which takes place on the α -carbon next to the NH group. As we show in this paper, the ESR analysis reveals a very small level of reactions that cannot be observed by common analytical methods, such as FTIR and NMR. As a next step, the elucidation of radical degradation mechanisms of PA in the presence of oxygen is also needed, and this work is currently underway.

Author Contributions: Conceptualization and methodology, A.K. and W.S.; simulation software and formal analysis, A.K.; resources, validation, investigation, and data curation, A.K. and W.S.; writing—original draft preparation, A.K., writing—review and editing, A.K., K.K., W.S. and N.T.; supervision, A.K., K.K., W.S. and N.T. All authors have read and agreed to the published version of the manuscript.

Funding: This research received no external funding.

Institutional Review Board Statement: Not applicable.

Data Availability Statement: Not applicable.

Acknowledgments: I would like to thank Rie Okubo and Kazuko Kamesawa of Asahi-Kasei corporation for GPC analysis.

Conflicts of Interest: The authors declare no conflict of interest and certify that they have no affiliations with or involvement in any organization or entity with any financial interest or non-financial interest in the subject matter or materials discussed in this manuscript.

References

1. Andrady, A.L. Microplastics in the marine environment. *Mar. Pollut. Bull.* **2011**, *62*, 1596–1605. [[CrossRef](#)]
2. Andrady, A.L. The plastic in microplastics: A review. *Mar. Pollut. Bull.* **2017**, *119*, 12–22. [[CrossRef](#)] [[PubMed](#)]
3. Isobe, A.; Iwasaki, S.; Uchida, K.; Tokai, T. Abundance of non-conservative microplastics in the upper ocean from 1957 to 2066. *Nat. Commun.* **2019**, *10*, 417. [[CrossRef](#)] [[PubMed](#)]
4. Halle, A.; Ladirat, L.; Martignac, M.; Mingotaud, A.F.; Boyron, O.; Perez, E. To what extent are microplastics from the open ocean weathered? *Environ. Pollut.* **2017**, *227*, 167–174. [[CrossRef](#)] [[PubMed](#)]
5. Lambert, S.; Wagner, M. Formation of microscopic particles during the degradation of different polymers. *Chemosphere* **2016**, *161*, 510–517. [[CrossRef](#)]
6. Naveed, K.-R.; Wang, L.; Yu, H.; Ullah, R.S.; Haroon, M.; Fahad, S.; Li, J.; Elshaarani, T.; Khan, R.U.; Nazir, A. Recent progress in the electron paramagnetic resonance study of polymers. *Polym. Chem.* **2018**, *9*, 3306–3335. [[CrossRef](#)]
7. Rånby, B.; Rabek, J.F. *ESR Spectroscopy in Polymer Research*; Springer: Berlin/Heidelberg, Germany, 1977; Volume 1.
8. Schlick, S. (Ed.) *Advanced ESR Methods in Polymer Research*; John Wiley & Sons, Inc.: Hoboken, NJ, USA, 2006.
9. Buettner, G.R. Spin Trapping: ESR parameters of spin adducts 1474 1528V. *Free Radic. Biol. Med.* **1987**, *3*, 259–303. [[CrossRef](#)]
10. Janzen, E.G.; Haire, D.L. ChemInform Abstract: Two Decades of Spin Trapping. *ChemInform* **1991**, *22*. [[CrossRef](#)]
11. Janzen, E.G.; Stronks, H.J.; Dubose, C.M.; Poyer, J.L.; McCay, P.B. Chemistry and Biology of Spin-Trapping Radicals Associated with Halocarbon Metabolism In Vitro and In Vivo. *Environ. Health Perspect.* **1985**, *64*, 151–170. [[CrossRef](#)]
12. Janzen, E.G. Spin trapping. *Acc. Chem. Res.* **1971**, *4*, 31–40. [[CrossRef](#)]
13. Sono, M.; Kinashi, K.; Sakai, W.; Tsutsumi, N. Spin-trapping analysis of thermal degradation reaction of poly(butylene terephthalate). *Macromolecules* **2017**, *50*, 254–263. [[CrossRef](#)]
14. Sono, M.; Kinashi, K.; Sakai, W.; Tsutsumi, N. Spin-Trapping Analysis and Characterization of Thermal Degradation of Thermoplastic Poly(ether-ester) Elastomer. *Macromolecules* **2018**, *51*, 1088–1099. [[CrossRef](#)]
15. Hayashi, T.; Kinashi, K.; Sakai, W.; Tsutsumi, N.; Fujii, A.; Inada, S.; Yamamoto, H. Spin-trapping analysis for thermal degradation of poly(vinyl alcohol). *Polymer* **2021**, *217*, 123416. [[CrossRef](#)]
16. Nguyen, T.A.; Ichise, S.; Kinashi, K.; Sakai, W.; Tsutsumi, N.; Okubayashi, S. Spin trapping analysis of the thermal degradation of polypropylene. *Polym. Degrad. Stab.* **2022**, *197*, 109871. [[CrossRef](#)]
17. Levchik, S.V.; Weil, E.D.; Lewin, M. Thermal decomposition of aliphatic nylons. *Polym. Int.* **1999**, *48*, 532–557. [[CrossRef](#)]
18. Pielichowski, K.; Njuguna, J. *Thermal Degradation of Polymeric Materials*; EngineeringPro Collection; iSmithers Rapra Publishing: Shropshire, UK, 2005.
19. Holland, B.J.; Hay, J.N. Thermal degradation of nylon polymers. *Polym. Int.* **2000**, *49*, 943–948. [[CrossRef](#)]
20. Schaffer, M.A.; Marchildon, E.K.; McAuley, K.B.; Cunningham, M.F. Thermal Nonoxidative Degradation of Nylon 6,6. *Macromol. Sci. Part C Polym. Rev.* **2000**, *C40*, 233–272. [[CrossRef](#)]
21. Ballistreri, A.; Garozzo, D.; Giuffrida, M.; Montaudo, G. Mechanism of thermal decomposition of Nylon 66. *Macromolecules* **1987**, *20*, 2991–2997. [[CrossRef](#)]
22. Herrera, M.; Matuschek, G.; Kettrup, A. Main products and kinetics of the thermal degradation of polyamides. *Chemosphere* **2001**, *42*, 601–607. [[CrossRef](#)]
23. Gonçalves, E.S.; Poulsen, L.; Ogilby, P.R. Mechanism of the temperature-dependent degradation of polyamide 66 films exposed to water. *Polym. Degrad. Stab.* **2007**, *92*, 1977–1985. [[CrossRef](#)]
24. El-Mazry, C.; Correc, O.; Colin, X. A new kinetic model for predicting polyamide 6-6 hydrolysis and its mechanical embrittlement. *Polym. Degrad. Stab.* **2012**, *97*, 1049–1059. [[CrossRef](#)]
25. El-Mazry, C.; Hassine, M.B.; Correc, O.; Colin, X. Thermal oxidation kinetics of additive free polyamide 6-6. *Polym. Degrad. Stab.* **2013**, *98*, 22–36. [[CrossRef](#)]

26. Catiker, E.; Guven, O.; Ozarslan, O.; Chipara, M. ESR investigations on γ -ray irradiated 3-methyl nylon 3. *Nucl. Instrum. Methods Phys. Res. B* **2008**, *266*, 3100–3106. [[CrossRef](#)]
27. Pagrk, J.B.; Devries, K.L.; Statton, W.O. Chain rupture during tensile deformation of nylon 6 fibers. *J. Macromol.Sci. Part B Phys.* **1978**, *15*, 205–227. [[CrossRef](#)]
28. Kausch-Blecken Von Schmeling, H.H. Application of Electron Spin Resonance Techniques to High Polymer Fracture. *J. Macromol. Sci. Part C: Polym. Rev.* **1970**, *4*, 243–280. [[CrossRef](#)]
29. Lee, S.S.; Phillips, P.J. Melt crystallized polyamide 6.6 and its copolymers, Part, I. Melting point—Lamellar thickness relations in the homopolymer. *Eur. Polym. J.* **2007**, *43*, 1933–1951. [[CrossRef](#)]
30. Konaka, R.; Terabe, S. Spin trapping of short-lived free radicals by use of 2,4,6-tri-*tert*-butylnitrosobenzene. *J. Am. Chem. Soc.* **1971**, *93*, 4306–4307. [[CrossRef](#)]
31. Yamada, B.; Fujity, M.; Sakamoto, K.; Otsu, T. Spin trapping of propagating radicals with 2,4,6-tri-*tert*-butyl-1-nitrosobenzene in radical polymerization initiated with di-*tert*-butyl hyponitrite. *Polym. Bull.* **1994**, *33*, 309–316. [[CrossRef](#)]
32. Qu, B.J.; Xu, Y.H.; Shi, W.F.; Rånby, B. Photoinitiated Cross-Linking of Low-Density Polyethylene. 7. Initial Radical Reactions with Model Compounds Studied by Spin-Trapping ESR Spectroscopy. *Macromolecules* **1992**, *25*, 5220–5224. [[CrossRef](#)]
33. Tabata, M.; Sohma, J.; Yamaoka, H.; Matsuyama, T. A spin-trapping study on crosslinks induced by γ -and neutron irradiations of *n*-eicosane. *Inter. J. Rad. App. Inst. Part C. Rad. Phys. Chem.* **1986**, *27*, 35–39. [[CrossRef](#)]
34. Richaud, E.; Diogo, O.O.; Fayolle, B.; Verdu, J.; Guilment, J.; Fernagut, F. Review: Auto-oxidation of aliphatic polyamides. *Polym. Degrad. Stab.* **2013**, *98*, 1929–1939. [[CrossRef](#)]
35. Arash, B.; Thijsse, B.J.; Pecenko, A.; Simone, A. Effect of water content on the thermal degradation of amorphous polyamide 6,6: A collective variable-driven hyperdynamics study. *Polym. Degrad. Stab.* **2017**, *146*, 260–266. [[CrossRef](#)]